R. Krishna[1]
J. M. van Baten[1]

[1] Van 't Hoff Institute for Molecular Sciences, University of Amsterdam, The Netherlands.

Research Article

A Molecular Dynamic Investigation of the Diffusion of Methane-Ethane and Methane-Propane Mixtures in Zeolites

Molecular Dynamic (MD) simulations were carried out to determine the Maxwell-Stefan (M-S) diffusivities, $Đ_i$, and self-diffusivities, $D_{i,self}$, of methane (C1), ethane (C2), and propane (C3) for a variety of molecular loadings, q_i, in three classes of zeolite topologies: (1) intersecting channels (MFI, ISV, BEA), (2) one-dimensional (1D) channels (AFI, TON, FER, MOR, LTL), and (3) cages separated by windows (FAU, LTA, ERI, CHA, DDR). The $Đ_i$ are strongly dependent on loading, decreasing to zero at saturation loading in all cases. For 1D channels, the decrease of $Đ_i$ with q_i is severe. For cages separated by narrow windows (LTA, ERI, DDR, CHA), the $Đ_i$ increase sharply with q_i before eventually reducing to zero at saturation loading. Correlation effects are reflected in the ratio of the self- to M-S diffusivity, $D_{i,self}/Đ_i$; this ratio is seen to be strongly dependent on the topology. Correlation effects are negligibly small in zeolite structures with cages separated by narrow windows. For binary C1–C2 and C1–C3 mixtures in both intersecting channel structures and 1D channels, the $D_{i,self}$ of the more mobile species, C1, is reduced significantly due to the presence of the more tardy C2 or C3. The mobility of the tardy species is enhanced due to the presence of the mobile C1. For cages separated by narrow windows, the inter-cage hops are practically independent and there is no accelerating or decelerating effects during mixture diffusion.

Keywords: Binary mixtures, Diffusion, Modelling, Molecular dynamics, Zeolites

Received: June 18, 2006; *accepted:* August 5, 2006

DOI: 10.1002/ceat.200600183

1 Introduction

In many process applications, it is important to estimate the rates of diffusion of mixtures within zeolites. For this purpose, the Maxwell-Stefan equations [1, 2] are commonly used to relate the flux of a species to its chemical potential gradient:

$$-\rho\frac{q_i}{RT}\nabla\mu_i = \sum_{\substack{j=1\\ j\neq i}}^{n}\frac{q_j N_i - q_i N_j}{q_{j,sat}Đ_{ij}} + \frac{N_i}{Đ_i}; \qquad i = 1, \ldots n \tag{1}$$

In Eq. (1), $Đ_i$ is the Maxwell-Stefan diffusivity of species i, q_i is the molar loading, $q_{i,sat}$ is the saturation capacity of species i, and $Đ_{ij}$ are the binary exchange coefficients. The saturation capacities, $q_{i,sat}$, can be obtained from the pure component sorption isotherms, provided that these are available up to saturation limits. The gradient of the chemical potentials can be related to the gradients in the loadings by defining a matrix of thermodynamic factors $[\Gamma]$:

$$\frac{q_i}{RT}\nabla\mu_i = \sum_{j=1}^{n}\Gamma_{ij}\nabla q_j$$
$$\Gamma_{ij} \equiv \frac{q_i}{f_i}\frac{\partial f_i}{\partial q_j} \tag{2}$$
$$i, j = 1, \ldots n$$

Estimation of the various diffusivities in Eq. (1) is not an easy task. There are about 180 different zeolite structures with varying pore geometry, topology, and connectivity [3]. These structures can be divided into three broad classes, following the classification suggested by Beerdsen et al. [4]. Zeolites such as MFI, ISV, and BEA are made up of nano-sized channels that intersect one another in a regular pattern (see Fig. 1). Zeolites

Correspondence: R. Krishna (r.krishna@uva.nl), Van 't Hoff Institute for Molecular Sciences, University of Amsterdam, Nieuwe Achtergracht 166, 1018 WV Amsterdam, The Netherlands.

© 2006 WILEY-VCH Verlag GmbH & Co. KGaA, Weinheim

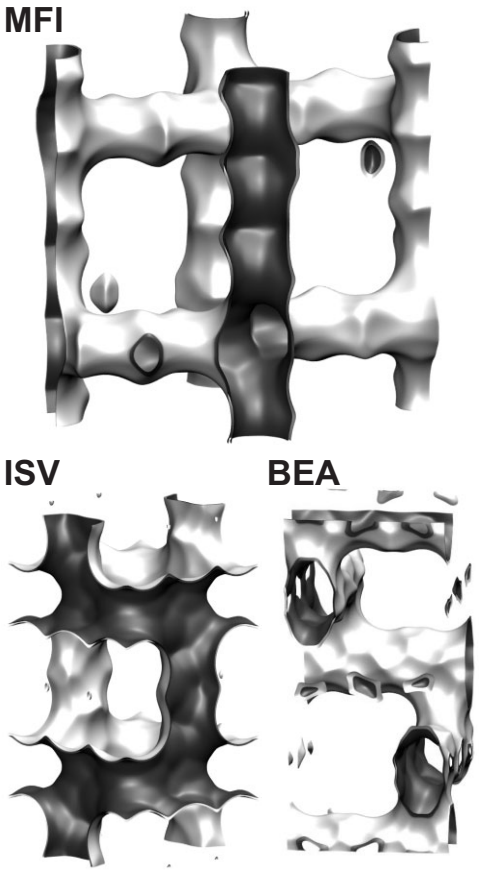

Figure 1. Zeolites with intersecting channel structures: MFI, ISV, and BEA.

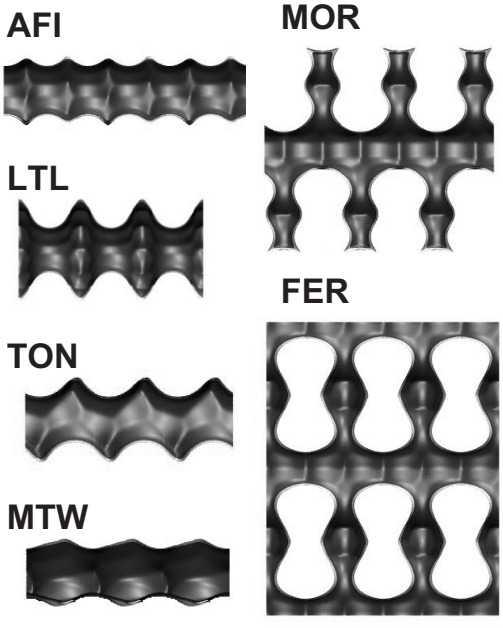

Figure 2. Zeolites with one-dimensional channel structures: AFI, MOR, MTW, TON, FER, and LTL.

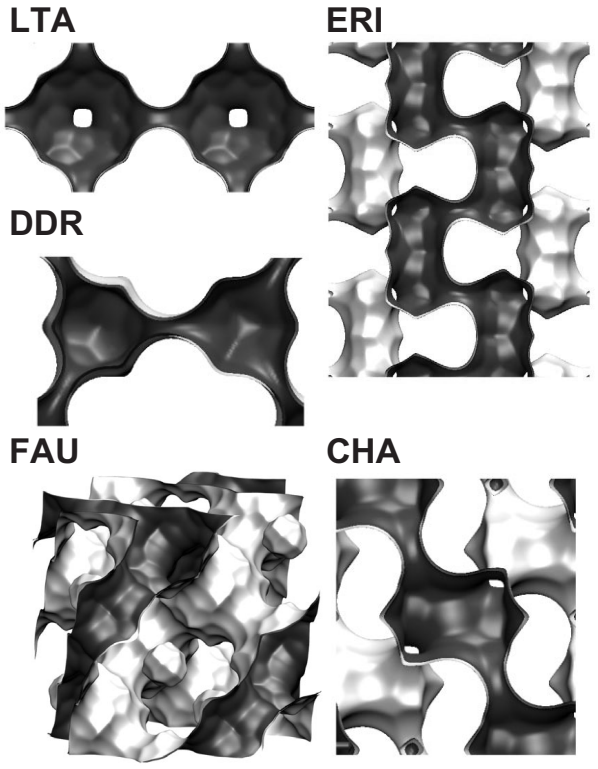

Figure 3. Zeolites structures consisting of cages separated by large windows (FAU) or narrow windows (LTA, CHA, DDR, ERI).

such AFI, MTW, TON, and LTL consist of one-dimensional (1D) channels (see Fig. 2). MOR and FER are also 1D channels but they are connected to side-pockets. The third category of zeolites consists of cage structures. The windows connecting the cages can be either wide, as in the case of FAU, or narrow as for LTA, CHA, DDR, and ERI (see Fig. 3).

The main objective of this paper is to compare the diffusion characteristics of the three classes of zeolite structures using Molecular Dynamic (MD) simulations. The MD simulation methodology, along with the force fields used, are described in earlier publications [1, 2, 5–11]; those details are not repeated here. We used methane (C1), ethane (C2), and propane (C3) as molecular probes, along with C1–C2 and C1–C3 equimolar mixtures.

2 Simulation Results and Discussion

In zeolites, the molecules are first adsorbed within the pores and motion within the zeolite is due to the adsorbed species which moves from one sorption site to another. Diffusion is closely inter-twined with the sorption behavior and it is necessary to first understand and describe mixture sorption. The adsorption isotherms can be calculated, most conveniently, by using Configurational-Bias Monte Carlo (CBMC) simulations as described in earlier studies [5]. For C1, C2, and C3, the adsorption strength of the pure component increases with the chain length, as shown for in Figs. 4a), 5a), and 6a) for MFI,

© 2006 WILEY-VCH Verlag GmbH & Co. KGaA, Weinheim

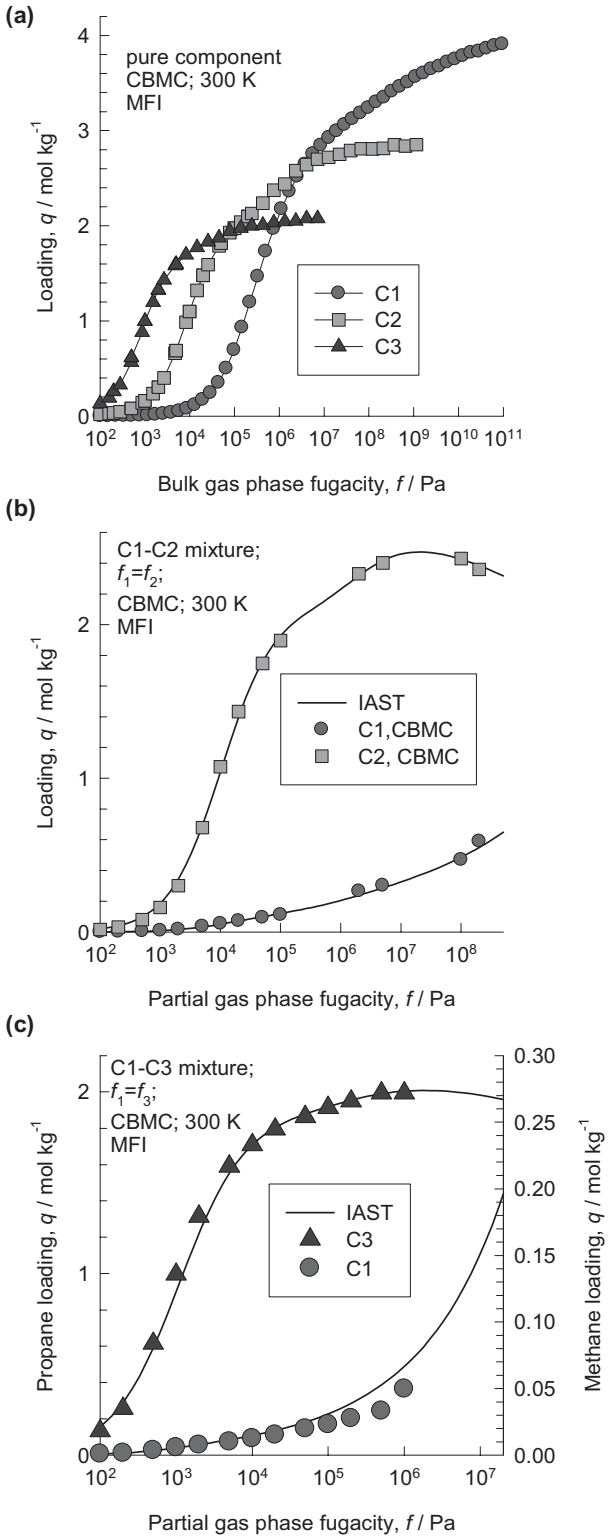

Figure 4. CBMC simulations of the sorption isotherms for (a) pure C1, C2, and C3, (b) C1–C2 mixture, and (c) C1–C3 mixture in MFI at 300 K. The continuous solid lines in (b) and (c) represent calculations with IAST [12] using 3-site Langmuir fits of pure component isotherms.

ISV, and AFI, respectively. In a mixture, the component with the higher adsorption strength has a higher loading; this can be seen for both C1–C2 and C1–C3 mixtures in Figs. 4b), 4c), 5b), and 6b). The smaller the alkane, the higher the saturation capacity, $q_{i,sat}$. Mixture sorption is governed by both adsorption strength and saturation capacity. For mixture adsorption as the occupancy increases, the smaller molecule finds it easier to locate within the vacant sites of the zeolites. As a result, there is a selectivity reversal as the total pressure is increased; this "size entropy" effect is demonstrated for both C1–C2 and C1–C3 mixtures in Figs. 4b), 4c), 5b), and 6b). For accurate prediction of mixture sorption from pure component isotherm data, we must use the Ideal Adsorbed Solution Theory (IAST) of Myers and Prausnitz [12]. The IAST predictions obtained from pure component sorption data are in reasonably good agreement with the CBMC simulation results for loading in mixture.

For flux calculations, we also need to determine the thermodynamic factors defined in Eq. (2). For single component dif-

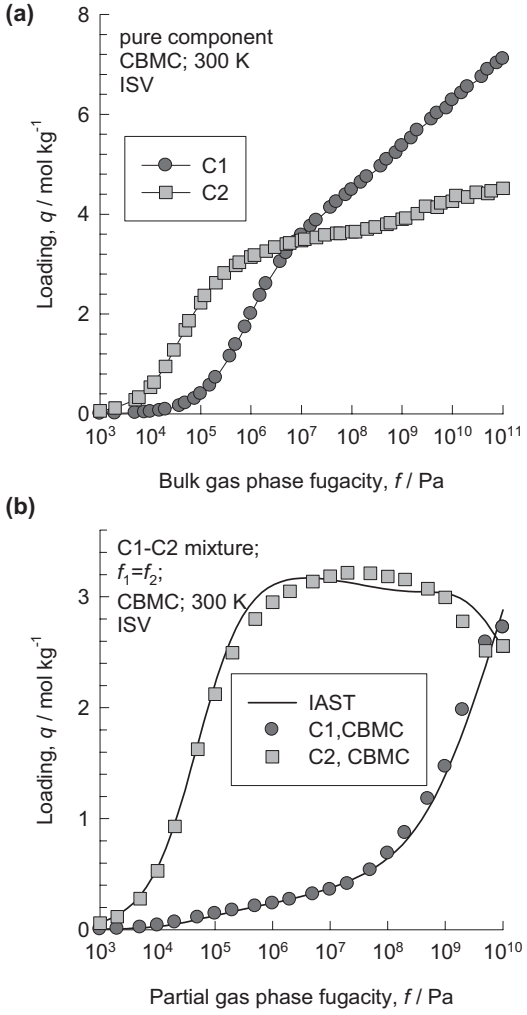

Figure 5. CBMC simulations of the sorption isotherms for (a) pure C1 and C2, and (b) C1–C2 mixture in ISV at 300 K. The continuous solid lines in (b) represents calculations with IAST [12] using 3-site Langmuir fits of pure component isotherms.

© 2006 WILEY-VCH Verlag GmbH & Co. KGaA, Weinheim

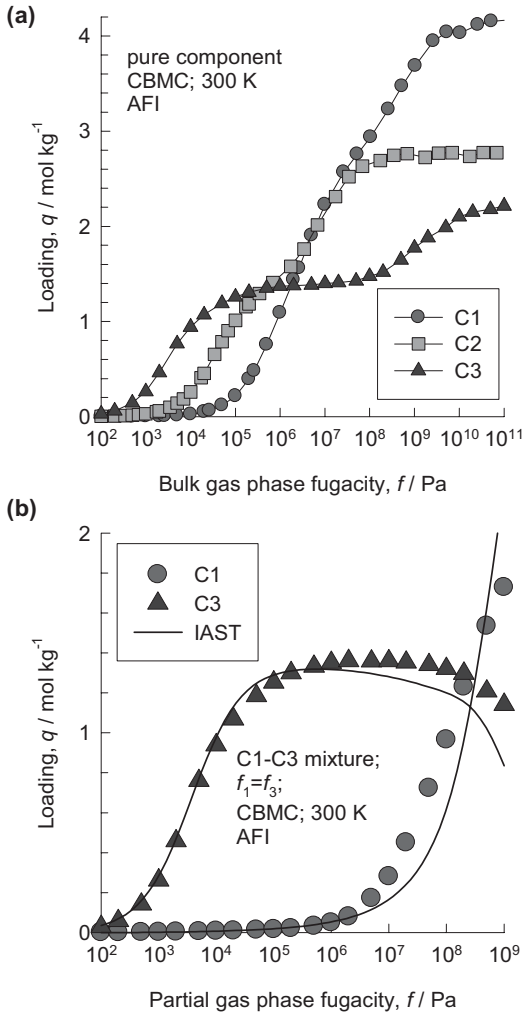

Figure 6. CBMC simulations of the sorption isotherms for (a) pure C1, C2, and C3, and (b) C1–C3 mixture in AFI at 300 K. The continuous solid lines in (b) represents calculations with IAST [12] using 3-site Langmuir fits of pure component isotherms.

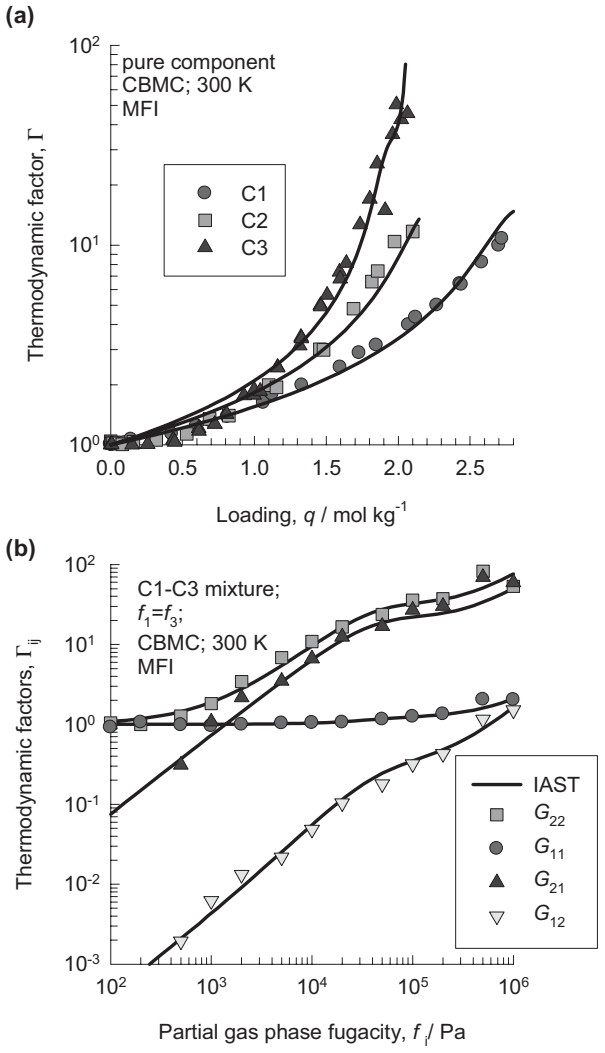

Figure 7. (a) Thermodynamic factor, Γ, determined from CBMC simulations of C1, C2, and C3 adsorption in MFI at 300 K, using the Reed and Ehrlich fluctuation formula, Eq. (3). (b) CBMC simulations using $[\Gamma]$ from Eq. (5) for C1–C3 mixtures in MFI at 300 K. The continuous solid lines represent calculations of $[\Gamma]$ with IAST [12] using 3-site Langmuir fits of pure component isotherms.

fusion, the Γ_i can be determined from CBMC simulations using the fluctuation formula of Reed and Ehrlich [8, 13, 14]:

$$\Gamma_i \equiv \frac{\partial \ln f_i}{\partial \ln q_i} = \frac{\langle n \rangle}{\langle n^2 \rangle - \langle n \rangle^2} \tag{3}$$

To illustrate this, we present in Fig. 7a) CBMC simulations of Γ_i for C1, C2, and C3, respectively, in MFI at 300 K. Also indicated by the continuous solid lines in Fig. 7a), are the calculations by the analytic differentiation of the isotherm fits; the agreement is very good. The fluctuation formula of Reed and Ehrlich [13] can be extended to a binary mixture to obtain the following expression for the inverse matrix of the thermodynamic factors, $[G]$:

$$G_{ji} \equiv \frac{f_i}{q_i}\frac{\partial q_j}{\partial f_i} = \frac{\langle n_i n_j \rangle - \langle n_i \rangle \langle n_j \rangle}{\langle n_i \rangle} \tag{4}$$

The desired elements of the matrix of the thermodynamic factors $[\Gamma]$ are obtained by matrix inversion:

$$[\Gamma] = [G]^{-1} \tag{5}$$

CBMC simulations of $[\Gamma]$ for C1–C3 mixtures in MFI at 300 K are shown in Fig. 7b), where Eq. (5) has been used. The continuous solid lines represent calculations of $[\Gamma]$ with IAST [12]. One concludes that the IAST is of reasonable accuracy when applied to process design calculations.

We turn to the estimation of diffusivities. The Maxwell-Stefan diffusivity, $Đ_i$, or "corrected" diffusivity [15] of both C1 and C2 in the three classes of zeolites, are shown in Figs. 8 and 9. For every zeolite structure, $Đ_i$ is seen to be a strong function of the molar loading q_i. Without exception, the $Đ_i$ reduce to zero at saturation loading $q_{i,sat}$. This was verified in every case by CBMC simulations of the pure component sorption isotherms up to saturation limits.

© 2006 WILEY-VCH Verlag GmbH & Co. KGaA, Weinheim

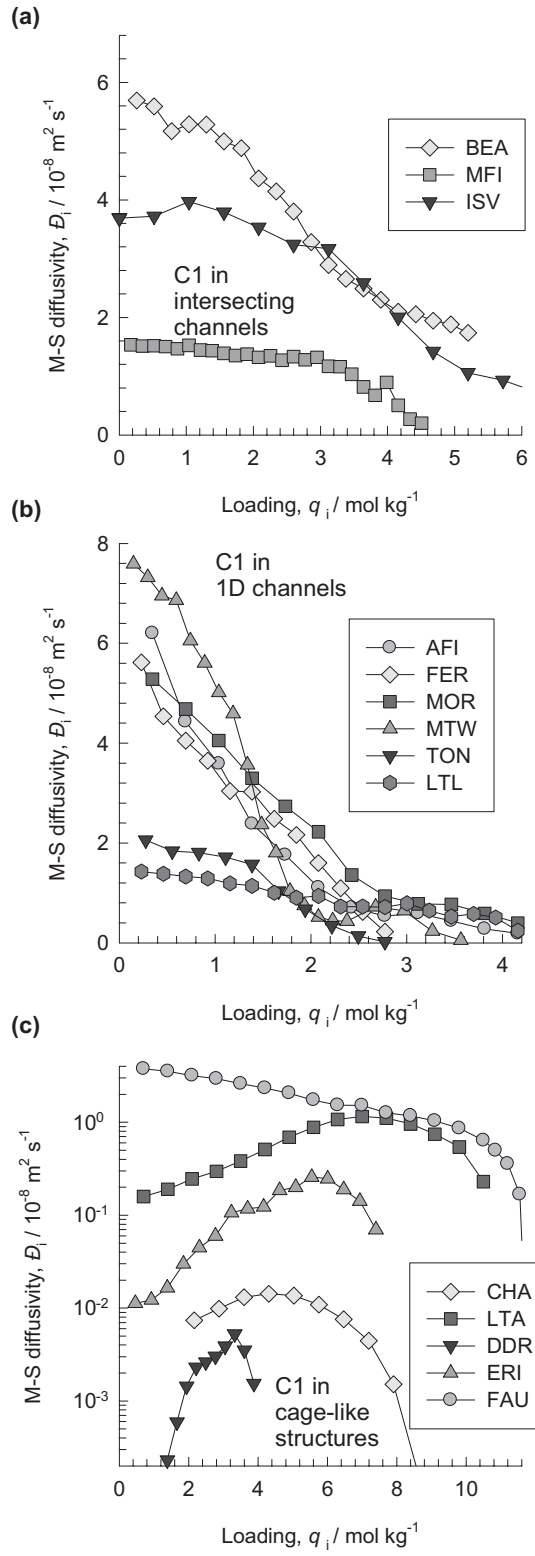

Figure 8. Loading dependence of the M-S diffusivity, $Đ_i$, of C1 in zeolites of three different topologies: (a) intersecting channel structures, (b) one-dimensional channels, and (c) cages connected by windows. The simulation results are for 300 K with the exception of LTA (750 K) and ERI (600 K).

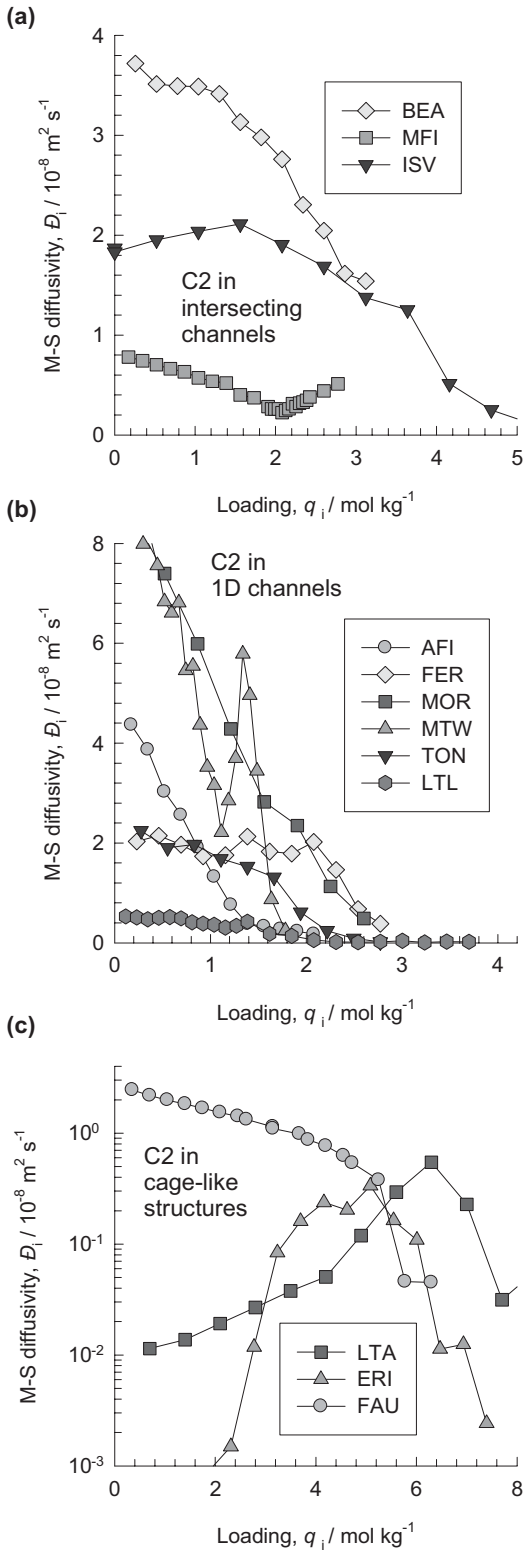

Figure 9. Loading dependence of the M-S diffusivity, $Đ_i$, of C2 in zeolites of three different topologies: (a) intersecting channel structures, (b) one-dimensional channels, and (c) cages connected by windows. The simulation results are for 300 K with the exception of LTA (750 K) and ERI (600 K).

© 2006 WILEY-VCH Verlag GmbH & Co. KGaA, Weinheim

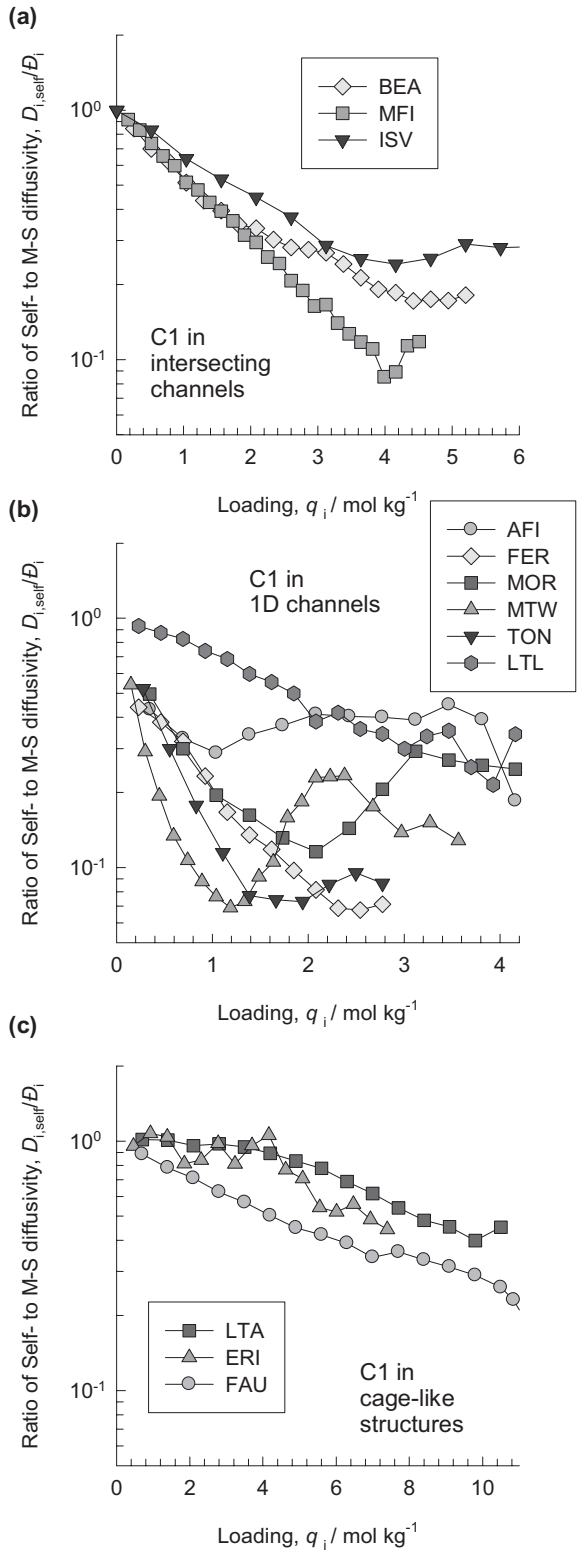

Figure 10. Ratio of the self-diffusivity to M-S diffusivity, $D_{i,self}/Đ_i$, of C1 in zeolites of three different topologies: (a) intersecting channel structures, (b) one-dimensional channels, and (c) cages connected by windows.

For 1D channel structures, the $Đ_i$–q_i dependence can be related to the loading dependence of the inverse of the thermodynamic correction factor Γ_i. As discussed in an earlier publication [8], for 1D channel structures as an approximation, the $Đ_i$–q_i dependence is proportional to that of $1/\Gamma_i$–q_i. In FAU, that has cages separated by wide windows, the $Đ_i$ decrease almost linearly with $(1-\theta_i)$, where

$$\theta_i = q_i/q_{i,sat} \quad i = 1, 2, \ldots n \tag{6}$$

is the fractional occupancy of species i [1, 16]. For cage structures separated by narrow windows (LTA, ERI, CHA, DDR), there is a sharp initial increase in $Đ_i$, followed by an inevitable decline to zero as saturation loading is approached. The increase in the $Đ_i$ with q_i is due to the reduction in the free energy barrier for inter-cage hopping of molecules caused by the increased free energy within a cage [4].

The M-S diffusivity $Đ_i$ reflects the collective motion of molecules, whereas the self-diffusivity, $D_{i,self}$, monitors the individual motions. A molecule can hop to a position that it had vacated earlier, and therefore, the jumps monitored are correlated. Due to correlation effects, the self-diffusivity is always smaller than the M-S diffusivity, i.e., $D_{i,self} < Đ_i$. The ratio $D_{i,self}/Đ_i$ is a measure of the strength of the correlations; the smaller the ratio, the greater the degree of correlation. Fig. 10 compares $D_{i,self}/Đ_i$ for C1 diffusion in different zeolites. We note that in general, the ratio $D_{i,self}/Đ_i$ decreases with increasing loading, or equivalently, the occupancy within the zeolite. As the occupancy increases, the probability that a molecule has to jump back to a position that it had vacated recently, increases due to the decreasing number of vacant sites. In zeolites with either intersecting or 1D channels, and in FAU that has cages separated by large windows, correlation effects are strong and $D_{i,self}/Đ_i$ reduces to values as low as 0.1.

For zeolites with cages separated by narrow windows (LTA, CHA, ERI, DDR), the ratio $D_{i,self}/Đ_i$ is close to unity, suggesting that the inter-cage jumps of molecules are practically independent of one another. An important consequence of this is that the diffusivity of a species, whether it is present on its own or in the presence of another species, remains unchanged. This is illustrated for LTA in Fig. 11, which compares the values of $D_{i,self}$ for pure C1, C2, and C3 with those in C1–C2 and C1–C3 mixtures, respectively. The comparison is made on the basis of the occupancy, which is defined for mixtures as:

$$\theta = \sum_{i=1}^{n} q_i/q_{i,sat} \tag{7}$$

A good approximation for diffusion in LTA, CHA, ERI, and DDR is to use the uncoupled flux relations

$$N_i = -\rho Đ_i \frac{q_i}{RT}\nabla\mu_i; \qquad i = 1, \ldots n \tag{8}$$

for mixture diffusion. Indeed, Eq. (8) which is a special case of Eq. (1), was used by Habgood [17] to describe mixture diffusion in LTA-4A. Our earlier re-analysis of the Habgood experimental data [18] has indeed yielded a good match with a model using Eq. (8) to describe mixture uptake.

For all zeolites other than those with cages and narrow windows, correlation effects tend to influence diffusion in mix-

© 2006 WILEY-VCH Verlag GmbH & Co. KGaA, Weinheim

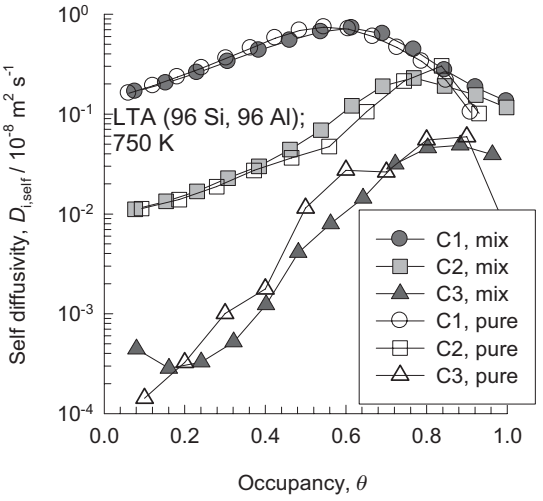

Figure 11. Comparison of $D_{i,self}$ of pure components C1, C2, and C3 with that in a C1–C2 and C1–C3 50–50 mixture in LTA at 750 K, respectively.

tures. Generally speaking, the more mobile species is slowed down and the tardy species is accelerated. We shall illustrate this by means of several examples. Fig. 12 compares $D_{i,self}$ of both pure C1 and C2 with that in a 50–50 C1–C2 mixture for the intersecting channel structures of (a) MFI, (b) ISV, and (c) BEA. Fig. 13 compares $D_{i,self}$ of pure C1 and C2 with that in a 50–50 C1–C2 mixture in (a) the 1D channels of FER and (b) FAU, which has cages separated by large windows. In all five cases, the $D_{i,self}$ of C1 is significantly lowered in the mixture; concomitantly C2 is accelerated. In the 1D channels of FER, the self-diffusivity of C1 and C2 in the mixture are closer together than in the other structures; this is due to the stronger correlation effects as witnessed from the data in Fig. 10.

The self-diffusion data for C1–C3 mixtures in MFI, AFI, and FAU are compared with the pure component values in Fig. 14; similar conclusions as that derived for C1–C2 can be drawn here. We note that in AFI, the diffusivities of C1 and C3 are close to one another. As an approximation, we may assume that the diffusivity of individual species in 1D channels such as AFI, FER, TON, and MTW are the same. This result also holds for diffusion in carbon nanotubes [2].

The stronger the correlation effect, the more pronounced is the deceleration and acceleration process in mixtures. In order to demonstrate this, we carried out simulations of the self-diffusivity in (a) C1–C2 and (b) C1–C3 mixtures in FAU, MFI, and BEA, keeping the total loading constant. These results are shown in Fig. 15, where the diffusivities in the mixture are normalized with respect to the pure component, $D_{i,self}$, at the same total loading. In the C1–C2 mixture, the C1 diffusivity decreases as the proportion of the more tardy C2 increases. Conversely, the diffusivity of C2 increases upon adding ever increasing amounts of the more mobile C1. The acceleration of C2 and deceleration of C1 are dependent on the zeolite topology, and is lower in BEA than in FAU and MFI. This is due to the weaker correlation effects. This can be verified by noting that the ratio $D_{i,self}/Đ_i$ is lower for BEA than for MFI; see Fig. 10a).

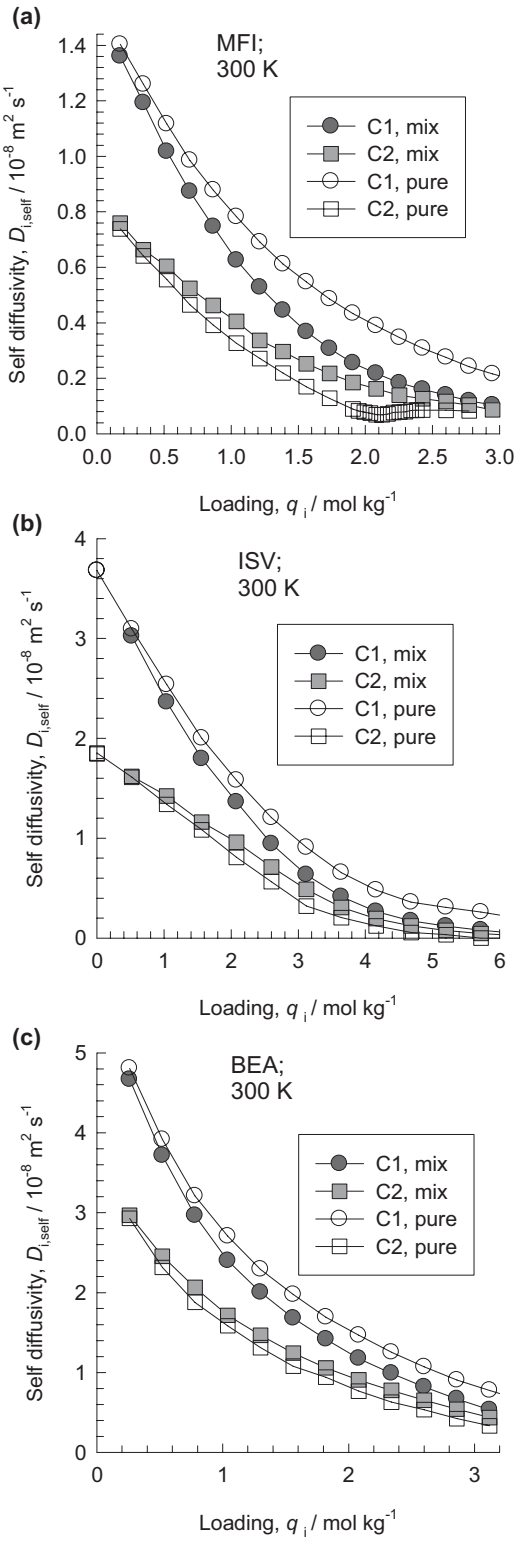

Figure 12. Comparison of $D_{i,self}$ of pure components, C1 and C2, with that in a 50–50 C1–C2 mixture in (a) MFI, (b) ISV, and (c) BEA.

© 2006 WILEY-VCH Verlag GmbH & Co. KGaA, Weinheim

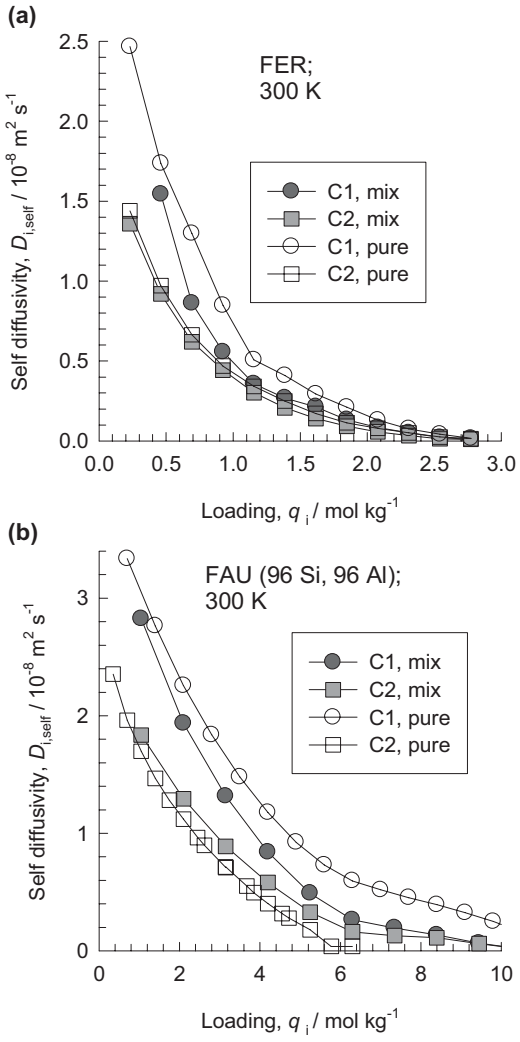

Figure 13. Comparison of $D_{i,self}$ of pure components, C1 and C2, with that in a 50–50 C1–C2 mixture in (a) FER and (b) FAU at 300 K.

For the C1–C3 mixtures, the acceleration and deceleration effects are more severe than for the C1–C2 mixtures. This can be deduced from the steeper slopes of the corresponding curves in Figs. 15a) and 15b).

3 Conclusions

The following conclusions can be drawn from the results presented in this paper:

– The M-S diffusivity, Đ$_i$, of C1 in zeolite structures is generally a strong function of loading and decreases to zero at saturation loading, $q_{i,sat}$. In zeolite structures consisting of cages separated by narrow windows (CHA, DDR, ERI, LTA), Đ$_i$ increases sharply with loading before decreasing to zero at $q_{i,sat}$. This increase in the diffusivity is due to the reduction in the free energy barrier for inter-cage hopping of molecules.

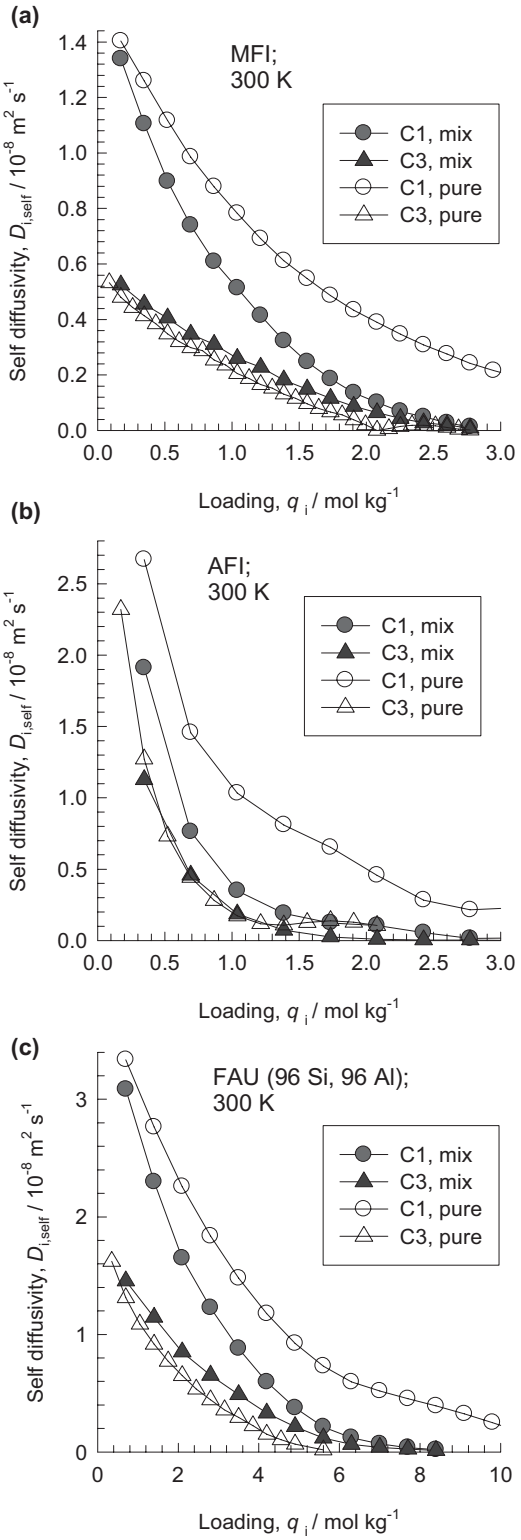

Figure 14. Comparison of $D_{i,self}$ of pure components, C1 and C3, with that in a 50–50 C1–C2 mixture in (a) MFI, (b) AFI, and (c) FAU at 300 K.

© 2006 WILEY-VCH Verlag GmbH & Co. KGaA, Weinheim

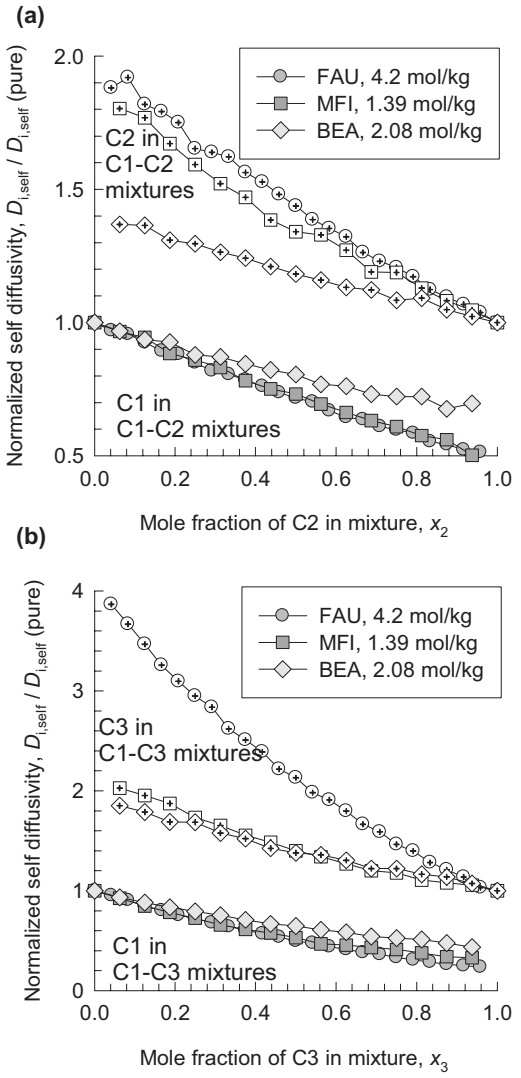

Figure 15. The self-diffusivity in mixture, normalized with respect to the value of the pure component at the same total loading, plotted versus the mole fraction in the mixture for (a) C1–C2 and (b) C1–C3.

– For zeolites with cages separated by narrow windows such as LTA, CHA, ERI, and DDR, the inter-cage hopping of molecules occur independent of one another. This implies that correlation effects are negligible and the diffusivity in a mixture is the same as that for pure components provided the comparison is made at the same total occupancy.
– For diffusion of mixtures within intersecting channels, within 1D channels, and in FAU, the more mobile species is slowed down and the tardy species is accelerated. The deceleration and acceleration is caused by correlation effects that increase with the occupancy within the zeolite.
– Correlation effects are particularly strong in 1D channel structures. Consequently, individual components in a mixture diffuse at roughly the same rate.
– The acceleration and deceleration are more severe for C1–C3 mixtures than for C1–C2 mixtures.

Acknowledgements

R. Krishna acknowledges the grant of a TOP subsidy from The Netherlands Foundation for Fundamental Research (NWO-CW) for the intensification of reactors and NWO/NCF for the provision of high performance computing resources.

References

[1] R. Krishna, J. M. van Baten, *J. Phys. Chem. B* **2005**, *109*, 6386.
[2] R. Krishna, J. M. van Baten, *Ind. Eng. Chem. Res.* **2006**, *45*, 2084.
[3] C. Baerlocher, L. B. McCusker, *Database of Zeolite Structures, http://www.iza-structure.org/databases/*, **2004**.
[4] E. Beerdsen, D. Dubbeldam, B. Smit, *Phys. Rev. Lett.* **2006**, *96*, 044501.
[5] D. Dubbeldam et al., *J. Phys. Chem. B* **2004**, *108*, 12301.
[6] R. Krishna, J. M. van Baten, *Chem. Phys. Lett.* **2005**, *407*, 159.
[7] R. Krishna, J. M. van Baten, *Ind. Eng. Chem. Res.* **2005**, *44*, 6939.
[8] R. Krishna, J. M. van Baten, *Chem. Phys. Lett.* **2006**, *420*, 545.
[9] R. Krishna, J. M. van Baten, *J. Phys. Chem. B* **2006**, *110*, 2195.
[10] J. M. van Baten, R. Krishna, *Microporous Mesoporous Mater.* **2005**, *84*, 179.
[11] J. M. van Baten, R. Krishna, *MD Simulations of Diffusion in Zeolites, http://www.science.uva.nl/research/cr/md/*, **2004**.
[12] A. L. Myers, J. M. Prausnitz, *AIChE J.* **1965**, *11*, 121.
[13] D. A. Reed, G. Ehrlich, *Surf. Sci.* **1981**, *102*, 588.
[14] H. Jobic et al., *J. Phys. Chem. B* **2006**, *110*, 2195.
[15] J. Kärger, D. M. Ruthven, *Diffusion in zeolites and other microporous solids*, John Wiley & Sons, New York, **1992**.
[16] S. Chempath, R. Krishna, R. Q. Snurr, *J. Phys. Chem. B* **2004**, *108*, 13481.
[17] H. W. Habgood, *Canad. J. Chem.* **1958**, *36*, 1384.
[18] R. Krishna, R. Baur, *Sep. Purif. Technol.* **2003**, *33*, 213.

© 2006 WILEY-VCH Verlag GmbH & Co. KGaA, Weinheim